



**Determination of
hydrology and erosion
model parameters:
Natural site adjacent to
Pit #1 at ERA Ranger
Mine, Northern Territory,
Australia**

Lyndon SJ Bell
Garry R Willgoose

January 1998



**Determination of Hydrology and Erosion Model Parameters -
Natural Site Adjacent to Pit #1 at ERA Ranger Mine Northern
Territory, Australia.**

by

Lyndon S.J. Bell & Garry R. Willgoose

**Department of Civil, Surveying and Environmental Engineering,
University of Newcastle
Callaghan NSW 2308**

January 1998

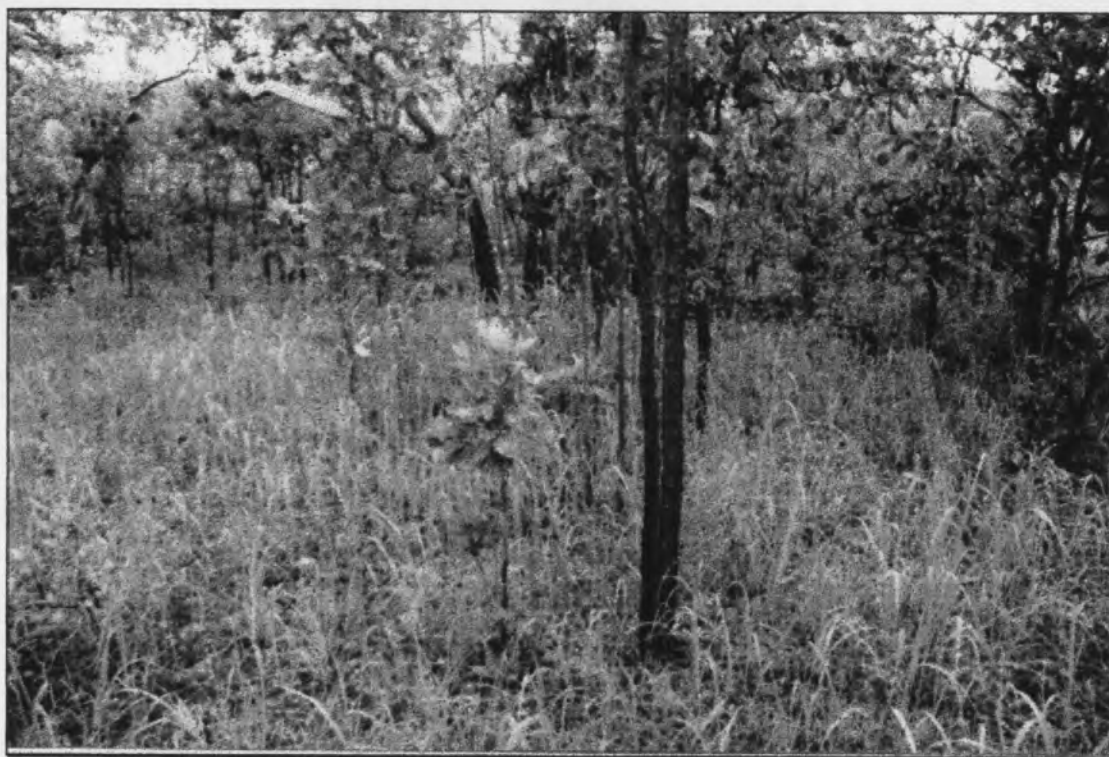
File Reference: JR-05-236



ENVIRONMENTAL RESEARCH INSTITUTE OF THE SUPERVISING SCIENTIST



ERA Ranger Mine, Pit 1.



Vegetation and ground-cover on undisturbed bushland beside Pit 1.

Acknowledgments

Acknowledgment is given to the invaluable support provided by my supervisor at the University of Newcastle, Dr. G. Willgoose, and my supervisor at *eriss*, Mr K. Evans (Senior Professional Officer, Erosion and Hydrology Section).

The support at *eriss* of Mr D. Moliere, Mr M. Saynor and Mr B. Smith, (Erosion and Hydrology Section) and Mr T. House and Mr T Mount (Information Technology Section) is also gratefully acknowledged.

Mr G. Cramb, ERA Environmental Services (ERAES) is thanked for his assistance and liaison between ERA Ranger Mine and *eriss*. Mr R. McAllister (ERAES) and Mr G. McKenzie (ERARM) are thanked for technical advice.

ERARM is thanked for the provision of; data-logging equipment, field plot construction materials, and earthmoving equipment.

My thanks are extended to Mr J Bell, Mr J Foster and Ms S Hickling, for their assistance in data acquisition and processing. Finally, the ANCA volunteers whom were involved in the initial construction of the field plot are thanked for their assistance.

Executive Summary

The current study involved erosion and hydrology data collection and parameter estimation on a 600 square metre field plot adjacent to Pit No. 1, at ERA Ranger Mine. Runoff and sediment loss data, resulting from natural rainfall, were collected during the 1996/1997 wet season and utilised to derive parameters for the Field Williams hydrology model, DISTFW; and the overland flow erosion and total sediment loss, sediment transportation models from the landform evolution model SIBERIA.

The kinematic wave and infiltrative loss parameters from DISTFW, were estimated from rainfall and runoff data utilising the non-linear regression analysis package NLFIT. The mean values for the DISTFW parameters were ascertained from eight storm events which had peak discharges in excess of 1 L/s, and a well defined duration. The mean values of the kinematic wave parameters C_r and e_m , were 4.98 and 1.82, respectively. The mean values of the infiltrative loss parameters S_ϕ and ϕ , were $1.67 \text{ mm/hr}^{1/2}$ and 14.55 mm/hr, respectively.

A comparison between DISTFW parameters obtained from the current study and the Tin Camp Creek study (comprising two field plots, the Quartz and Mica sites) was undertaken to ascertain if there were any differences in modelled hydrological behaviour. A 95% posterior probability comparison of kinematic wave parameters from eight individual storm events from the current study, and four storm events (compressed into only two sets of parameters) from both the Mica and Quartz sites, highlighted no conclusive trends, even though the Quartz site was considered to be a possible outlier. The comparison of the infiltrative loss parameters between four individual storms from the current study, and the two sets of parameters from the Mica and Quartz sites, highlighted that the Mica site was notably outside the general trend and was considered to be significantly different.

Sediment transportation rate estimation on the natural site was quantified with two similar models; the overland flow erosion; and the total sediment loss models.

The overland flow erosion model is of the form.

$$Q_s = \beta_1 W^{(1-m_1)} Q^{m_1} S^{n_1}$$

The parameters of the overland flow erosion model were estimated from a regression analysis utilising all of the collected suspended sediment experimental data from eight observed storm events.

$$Q_s = 0.917 W^{(1-0.854)} Q^{0.854} S^{0.69} \quad (r^2=0.74, df=169, p<0.001)$$

The total sediment loss erosion model is of the form.

$$T = \beta_1 W^{(1-m_1)} S^{n_1} \int Q^{m_1} dt$$

The parameters of the total sediment loss model were estimated from a regression analysis utilising both the bedload and suspended sediment experimental data from five significant storm events.

$$T = 1.171 W^{(1-1.120)} S^{0.69} \int Q^{1.120} dt \quad (r^2=0.99, df=4, p<0.001)$$

The magnitude of the erosion parameters β_1 and m_1 , from the current study compare well to previous studies on the Northern Waste Rock Dump of ERARM and in the Tin Camp Creek area, and enables quantification of the trend that the exposed waste rock material will experience decreasing rates of erosion over time.

Table of Contents

<i>Acknowledgments</i>	<i>ii</i>
<i>Executive Summary</i>	<i>iii</i>
<i>Table of Contents</i>	<i>v</i>
<i>List of Figures</i>	<i>vii</i>
<i>List of Tables</i>	<i>x</i>
1.0 Introduction	1
1.1 General Overview	1
1.2 Erosion and Hydrology	3
1.3 Research Objectives	6
2.0 Rainfall-Runoff Experimental Field Plot	11
2.1 General Overview	11
2.2 Experimental Field Plot	14
3.0 DISTFW-NLFIT Rainfall-Runoff Model	24
3.1 Introduction	24
3.2 DISTFW-NLFIT	27
3.2.1 Infiltration	27
3.2.2 Routing of Overland Flow - Hillslope Run-off	32
3.2.3 Routing of Channel Flow	34
3.3 DISTFW Data Requirements	39
3.4 DISTFW-NLFIT Calibration Procedure	45
3.5 NLFIT-General and Least Squares Error Models	48
3.6 Data	54
3.7 Parameter Comparison	63

4.0 Sediment Transport Model Parameter Fitting	75
4.1 Introduction	75
4.2 Sediment Transportation Models	76
4.3 Data	78
4.4 Parameter Comparison	86
5.0 Evaluation of the Effect of Vegetation Growth Over Wet Season	90
6.0 Further Work	97
7.0 References	98

Appendix 3.A: DISTFW Rainfall and Runoff Input Files and Predicted Versus Observed Output Hydrographs and Accompanying Statistics.

Appendix 4.A: Suspended and Bedload Sediment Data and Sample Processing Procedure.

Appendix 4.B: Particle Size Analysis.

Appendix 4.C: Regression Analysis for Overland Flow Erosion and Total Sediment Loss Models.

List of Figures

Figure 1.1.1: The locality of ERARM within the Northern Territory. The mine-site is approximately 270 kilometres East of Darwin (after Finnegan, 1993).	2
Figure 1.2.1: Mean monthly rainfall and evaporation at Jabiru Airport, approximately 5 kilometres West of ERARM (after Finnegan, 1993).	3
Figure 1.3.1: Each study listed is assumed to represent the weathered state of waste rock material after a certain number of years of exposure.	7
Figure 1.3.2: The 4 square kilometre, 17 metre high post-mining rehabilitation structure prior to erosion commencement is featured at the top of this Figure. Featured at the bottom of this Figure is the landform after 1000 years of simulated erosion by SIBERIA (after Willgoose and Riley, 1993). The initiation of gully erosion is also highlighted in this Figure.	9
Figure 2.1.1: The undisturbed natural field plot is approximately 50 metres from the edge of Pit No. 1, ERARM. The eriss staff member featured in the background of this Figure, is standing along the access road.	11
Figure 2.1.2: Schematic diagram highlighting the position of the field plot relative to the SWRD, Pit No.1, and the access road. The large cross, indicates the position of Figure 2.1.1. The position of the drainage channel and raingauge that were installed during the monitoring program are also featured in this Figure.	12
Figure 2.1.3: Three dimensional topographic surface of the 30m by 20m erosion and hydrology field plot which collected both surface run-off and transported sediment at the downslope end of the plot with a 300mm diameter PVC pipe. The dimension listed on the x, y, and z axes are a function of the computer program and are only relative to each other.	13
Figure 2.2.1: The 20 cm wide bituminous aluminium building product, (damp-coarse), was bent in a letter 'L' shape, and nailed to the soil surface, and supported with concrete. The field plot was thus hydraulically isolated from the surrounding bushland.	14
Figure 2.2.2: One half of a 300 mm diameter, 20 m long PVC pipe was buried at the down-slope end of the field plot. Additional damp-coarse material was attached to the PVC pipe to prevent overflow of surface runoff. A concrete lip was installed to allow unhindered transport of sediment and surface runoff into the PVC pipe.	15
Figure 2.2.3: Featured in the foreground is the trapezoidal hydraulic control structure which was connected to a concrete reservoir which accumulated sediment, and partially controlled the run-off.	16
Figure 2.2.4: The concrete reservoir was served a dual purpose; to collect bedload sediment that was transported during rain events and steady the flow entering the weir. Surface runoff that is leaving the PVC pipe, (highlighted by a large arrow to the left of the Figure), enters the concrete reservoir and is quickly steadied.	17
Figure 2.2.5: The concrete reservoir serves as an aid to steady the flow of water across the trapezoidal weir, and as a storage area for bedload sediment.	18
Figure 2.2.6: Considerable quantities of surface run-off are transported from the field plot, the change in direction of flow, and the length of the reservoir both serve to control and steady the flow.	18
Figure 2.2.7: Cross-sectional view of the hydraulic control structure, with a base of 150 mm. The depth of water, with respect to cross-sectional area, is utilised to determine the discharge through the structure.	19
Figure 2.2.8: Run-off is still occurring in the foreground of this Figure after a storm event. The position of the hydraulic inlet that is connected to the stilling well containing the water level sensing device is also featured in this Figure.	20
Figure 2.2.9: Featured to the left of this Figure is the discharge trench that was constructed to carry runoff away from the experimental area. Attached to the star picket in the background of this Figure is the manual raingauge, and the steel cylinder sitting atop a pedestal, in the middle of the Figure, is the electronic tipping bucket raingauge.	22
Figure 2.2.10: A schematic of a tipping bucket raingauge featuring two L-shaped plastic buckets in a back to back configuration attached to a fulcrum, a magnet attached to the plastic bucket mechanism, and a magnetic sensitive switch which was connected to an electronic data logger.	23
Figure 3.1.1: Numerous mechanisms for water movement exist on hill-slopes including overland and subsurface pathways (after Gerrard, 1981).	24

Figure 3.1.2: Four module conceptual arrangement of the rainfall-runoff model, DISTFW, incorporating non-linear surface and linear groundwater storage, and kinematic wave hillslope and channel routing (after Willgoose et al, 1995).	26
Figure 3.2.1: Typical infiltration rate curves for different soil matrix compositions under ponded infiltration (Gerrard, 1981).	27
Figure 3.2.2: The infiltration envelope highlighted in this Figure, defines the time to ponding for rainfalls of different hypothetical intensities (Smith, 1972; cited in Kirkby and Morgan, 1980).	29
Figure 3.2.3: Incremental precipitation rate and its dissociation into amounts of infiltration, depression storage, and overland flow (Fetter, 1994).	31
Figure 3.2.4: A schematic of a hillslope which illustrates the principal of temporary storage of surface run-off, infiltration and subsurface flow (Kuczera 1996).	34
Figure 3.2.5: Combination of four different cross sectional profiles illustrating A) Constant depth sheet flow, B) Irregular depth sheet flow, C) Triangular rill flow, and D) Irregular depth rill flow (after Willgoose and Kuczera, 1995).	37
Figure 3.3.1: Regression analysis of the results obtained from the calibration experiment performed on the water level sensing device (capacitance rod), prior to installation on-site.	39
Figure 3.3.2: An extract from a raw data file unloaded from the UNIDATA data-logger highlighting the number of tips from the electronic raingauge, and the water level via a capacitance reading. It should be noted that the number in the column after the 'D', representing a data-entry line, represents the channel that each device was connected to within the data-logger.	40
Figure 3.3.3: The 30 m in length, and 20 m in width, 600 m ² field plot was divided into ten equally proportioned sub-catchments and upstream and downstream elevation information was entered into the 'Field Williams' file. The Northing and Eastings including topographic measurements can only be conservative to one another.	42
Figure 3.3.4: A typical Field Williams input file, containing topographic information on the field plot, and the rainfall and runoff input file names for a particular storm event.	43
Figure 3.3.5: A DISTFW rainfall input file featuring a title, and cumulative rainfall with accompanying time stamp in decimal hours since the commencement of the event.	44
Figure 3.3.6: A DISTFW runoff input file featuring a title, and discharge, (m ³ /s), with accompanying time stamp in decimal hours since the commencement of the event.	44
Figure 3.4.1: The global optimisation of the objective function $\psi(\gamma)$, involves the search vector moving in a down-gradient direction until a minimum is reached, denoted by an 'X' (Kuczera, 1994).	45
Figure 3.5.1: Plot of standardised residuals versus predicted response for a least squares model of the 1 st January 1997 event. The increasing spread of standardised residuals versus predicted response indicates that the residual variance is increasing with predicted response thus violating the least squares model assumption. The number 'X' in this plot refers to 'X' residuals occupying virtually the same position.	49
Figure 3.5.2: Plot of time versus standardised residuals for the 1 st January 1997 event. The Z statistic being -9.5, exceeds the test value of 2 , indicating that the standardised residuals are not independent.	50
Figure 3.5.3: A normal probability plot for the storm event occurring on the 1 st January 1997 with a Kolmogorov-Smirnov statistic of 0.1091, and a 5% exceedance value of 0.0690. As the Kolmogorov-Smirnov statistic exceeds the 5% test value, the residuals are considered not to be normally distributed.	51
Figure 3.5.4: Residual autocorrelation plot for the 1 st January storm event, which highlights the time dependence of the residuals, in this case the assumption of the residuals being statistically independent is not consistent with the data.	52
Figure 3.5.5: Residual cumulative periodogram plot for the 1 st January 1997 storm event, which should be linear assuming that the residuals are independent and constant (an assumption of the least squares error model).	53
Figure 3.6.1: Observed and predicted discharge, (m ³ /s), and cumulative rainfall, (mm), for the storm event occurring on the 1 st January 1997. The large arrow indicates a reduction in rainfall that resulted in a subsequent decrease in observed and predicted discharge from the field plot.	56

Figure 3.6.2: The ill-defined duration of the overnight storm event occurring over the 23 rd -24 th January, resulted in the considerable differences between the observed and predicted hydrographs.	57
Figure 3.6.3: The predicted hydrograph of the storm event occurring on the 19 th February, does not compare well with the observed hydrograph. Considerable fluctuation in the observed hydrograph over an extended period of time virtually negates the possibility of a smooth predicted response curve.	60
Figure 3.6.4: The inclination limb of the storm event occurring on the 28 th January, is well estimated, with a slight drop in discharge resulting from a fluctuation in rainfall, highlighted by an arrow. The recession limb is dominated by fluctuations in the observed hydrograph, highlighted by an arrow, resulting from intermittent rainfall occurring at the 1.5 hour mark.	61
Figure 3.6.4: The inclination limb of the second storm event of the 21 st January is adequately fitted, however the peak and the recession limb is poorly approximated. A large second discharge peak is predicted at the 0.5 hour mark and considerable under-prediction is evident beyond the 0.75 hour mark.	62
Figure 3.7.1: 95% posterior probability plot of the kinematic wave parameters, C , and e_m for the ten storm events listed from the current study and two parameter sets from the Mica and Quartz sites (Table 3.7.1).	69
Figure 3.7.2: The predicted hydrograph for the storm event occurring on the 4 th January, exhibits considerable deviation from the observed hydrograph in both the peak and the recession limb. Differences in the volume of the predicted hydrograph compared to that which was observed is believed to have been the origin of the large standard deviations of the infiltrative loss parameters listed in Table 3.7.2 for this event.	70
Figure 3.7.3: The end of predicted hydrograph for the storm event occurring on the 22 nd February was non-zero, due to an error in the DISTFW runoff input file. This was believed to have resulted in difficulties in the estimation of the volume of the hydrograph which was translated into large standard deviations for the infiltrative loss parameters, S_p and ϕ .	72
Figure 3.7.4: The predicted hydrograph for the storm event occurring on the 23 rd February, exhibits considerable deviation from the observed hydrograph in both the peak and in the recession limb. Differences in the volume of the predicted hydrograph compared to that which was observed is believed to be the origin of the large deviations of the infiltrative loss parameters, S_p and ϕ .	73
Figure 3.7.5: 95% posterior probability plot of the infiltrative parameters, S_p and ϕ , for four storm events from the natural site, 1 st and 3 rd January, 20 th and 22 nd pm February, and the Quartz and Mica sites from Tin Camp Creek.	74
Figure 4.3.1: Plot of the suspended sediment concentration, (g/L), and discharge, (m^3/s), versus time, (hours), for a storm event occurring on the 1 st January 1997.	79
Figure 4.3.2: A log-log regression analysis of ' Q ', discharge, (L/s), versus ' Q_s ', sediment discharge, (g/s), Equation (4.3.2), was performed utilising all the suspended sediment samples from eight storm events (Table 4.3.1).	80
Figure 4.3.3: A log-log regression analysis of the integration of $Q^{m1} dt$, (L^{m1}), against the total sediment loss, ' T ', (g), was performed utilising the five storm events listed in Table 4.3.2.	84
Figure 5.1: Natural field plot, 5 th December 1996.	90
Figure 5.2: Natural field plot, 30 th December 1996.	91
Figure 5.3: Natural field plot, 29 th January 1997.	91
Figure 5.4: Decomposing leaf litter from the previous wet season slowly breaks down during the course of the year and provides considerable coverage of the soil surface.	92
Figure 5.1: 95% posterior probability plot of the kinematic wave parameters C , and e_m for the eight storm events listed in Table 5.1. The eight storm events were divided into two groups, those occurring at the start and at the end of the wet season, each with their on defined mean.	94
Figure 5.2: Plot of the S_p values fitted from DISTFW-NLFIT, for eight storm events that occurred over the wet season that are listed in Table 5.1.	95
Figure 5.3: Plot of the ϕ values fitted from DISTFW-NLFIT, for eight storm events that occurred over the wet season that are listed in Table 5.1.	96

List of Tables

<i>Table 3.4.1: DISTFW model parameter initial calibration magnitudes and designation as to whether an estimation of the parameter was sought or whether the parameter's value was permanently fixed.</i>	46
<i>Table 3.6.1: Recorded storm events during the 1996/1997 wet season with associated total rainfall, (mm), peak discharge, (L/s) and storm duration (hours).</i>	54
<i>Table 3.6.2: Summary of infiltration and kinematic wave parameter values for all storm events that had a peak discharge in excess of 1L/s, and a definite storm duration.</i>	58
<i>Table 3.7.1: Mean and standard deviations for the kinematic wave and infiltrative loss DISTFW parameters for all the storm events from the current study listed in Table 3.6.2 (neglecting 22/1/97nd, 23-24/1/97, and 28/1/97) and the Tin Camp Creek study (Moliere et al, 1996).</i>	64
<i>Table 3.7.2: Summary of infiltration and kinematic wave parameter values for eight representative storm events from the natural site and from the Tin Camp Creek study.</i>	68
<i>Table 4.3.1: Storm events and respective rainfall and runoff characteristics for eight monitored storm events from the natural site.</i>	78
<i>Table 4.3.2: Eight observed storm events from the natural site and their respective total runoff, (L), total suspended and bedload sediment, (g).</i>	83
<i>Table 4.4.1: Comparison between the fitted erosion parameters β_1 and m_1, from the overland flow erosion and the total sediment loss model.</i>	86
<i>Table 4.4.2: Comparison between the fitted erosion parameters β_1 and m_1, from the overland flow erosion model for the Tin Camp Creek, utilising the complete data set, and data with discharge values less than 10L/s, and the natural site study.</i>	86
<i>Table 4.4.3: Comparison between the fitted erosion parameters β_1 and m_1, from the total sediment loss model for studies conducted on the Northern Waste Rock Dump, in the Tin Camp Creek area, and the current study.</i>	87
<i>Table 5.1: Summary of kinematic wave parameter values for eight storm events from the current study that occurred at the start of January and the end of February.</i>	93

1.0 Introduction

1.1 General Overview

The Energy Resources of Australia Ranger Mine (ERARM), is situated approximately 11 kilometres East of the township of Jabiru, enclosed by, but not a part of, the world heritage listed Kakadu National Park, in the Northern Territory. The mine-site is approximately 270 kilometres East of Darwin and occupies a 78 square kilometre lease, which incorporates both the current Ranger operation and the future Jabiluka operation (Figure 1.1.1).

The landscape within the Kakadu National Park is diverse and contrasting, ranging from the massive sandstone escarpment of the Arnhem land plateau, to flat open woodland, to expansive wetlands and billabongs that spill into the coastal fringe.

The Commonwealth body, the Office of the Supervising Scientist, of which the Alligator Rivers Region Research Institute (ARRRI) was a part of, was established to monitor and assess the environmental impact of the uranium mine on the surrounding environment. The ARRRI was renamed in 1993 as the Environmental Research Institute for the Supervising Scientist (*eriss*), (which is now a part of the Commonwealth Environment Department), from amendments to the Environmental Protection (Alligators Rivers Region) Act, (1978), to reflect the broadened role of the organisation. The program of research at *eriss*, is broadly outlined in Johnston (1995), and includes; the impact of mining on the environment, the protection and management of wetlands, and general environment protection research.

The Erosion and Hydrology Section at *eriss* has focussed, in recent years, on landform evolution modelling, which requires the input of data concerning the erosion and hydrology of such landforms (Johnston, 1995).

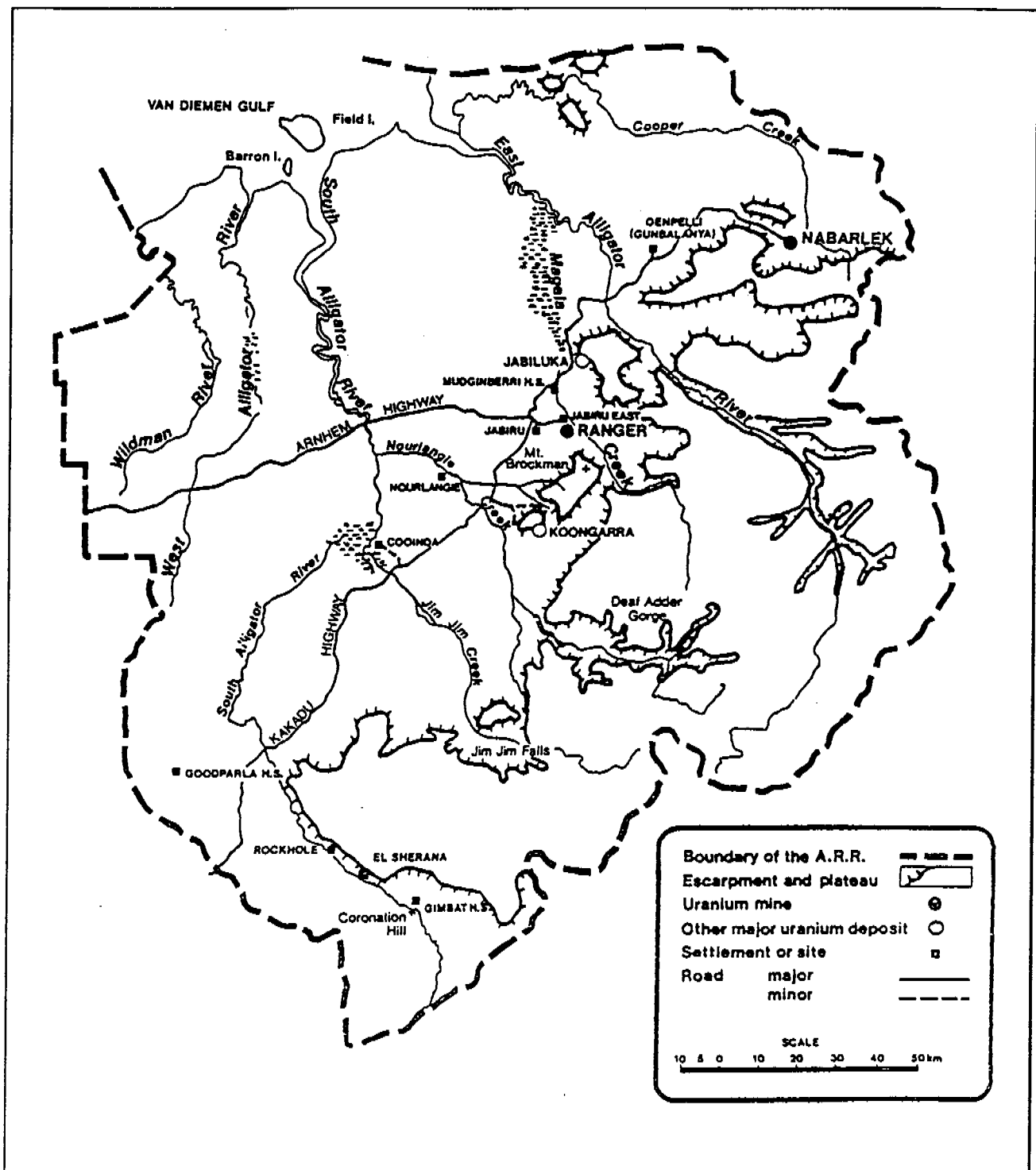


Figure 1.1.1: The locality of ERARM within the Northern Territory. The mine-site is approximately 270 kilometres East of Darwin (after Finnegan, 1993).

1.2 Erosion and Hydrology

The climatic fluctuations that occur within the Kakadu National Park are regarded as extreme. The annual rainfall characteristics of the region can be divided into distinct wet and dry seasons. The average temperature fluctuates between 25-35°C in the wet season and 17-30°C in the dry season. The wet season is characterised by a three to four month period of intensive rainfall from November to March, followed by the extended dry season, from April to October (Figure 1.2.1).

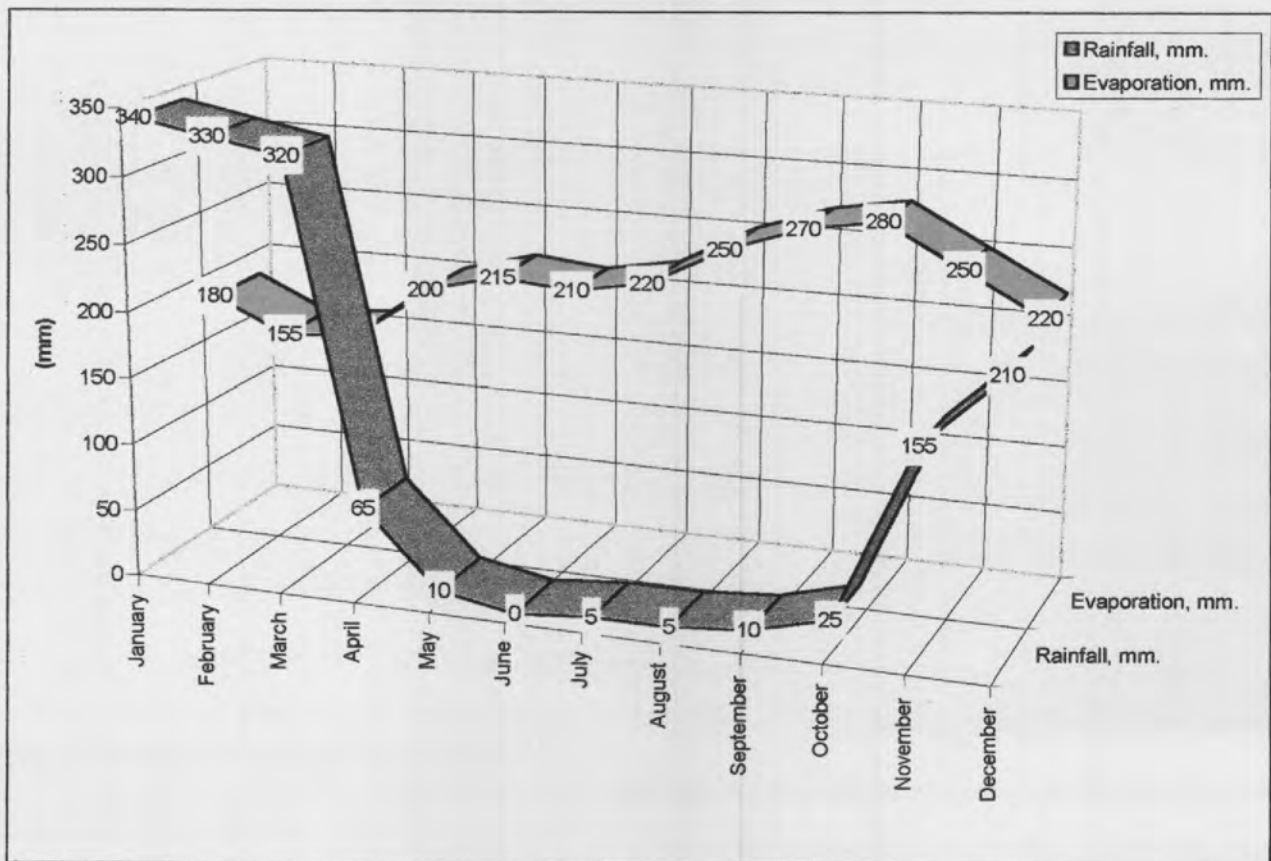


Figure 1.2.1: Mean monthly rainfall and evaporation at Jabiru Airport, approximately 5 kilometres West of ERARM (after Finnegan, 1993).

It can be observed from Figure 1.2.1, that the rates of evaporation across the year are fairly consistent, and that approximately 60% of the average annual rainfall of 1481 mm (20 year average) falls during the period January to March.

The distinct extremes between the wet and dry seasons of the region, has a considerable influence on the erodibility of the landscape. During the 1996/1997 wet season for example, considerable periods of intensive rainfall were noted, such as 60 mm of rainfall in less than one hour at the start of January, and 40 mm in just 18 minutes at the end of January.

In contrast, during the long periods of the dry season where there is virtually no rainfall, considerable quantities of sediment accumulate on the surface from accelerated weathering believed to be due to large temperature fluctuations between the day and night and the highly weatherable nature of the soil material.

The quantity and intensity of surface run-off is a major function governing sediment transportation (Willgoose and Riley, 1993). The magnitude of rainfall intensities previously reported, highlights the considerable potential for surface erosion in the region from rainfall.

ERARM exploits a stratabound uranium deposit hosted by the lower member of the Early Proterozoic Cahill Formation (Evans, Willgoose and Riley, 1995). The waste rock material from the ERARM operation comprises of carbonates, carbonaceous schists and mica, and quartz feldspar schist from that lower member (Needham, 1988; cited in Evans *et al*, 1995). Milnes (1988; cited in Evans, *et al*, 1995) noted that this waste rock material is highly weatherable, and large components of the chloritic schist fragments break down into medium and fine gravel and clay rich detritus within a two to three year period.

Willgoose and Riley (1993) noted that by circa 2012, when the all economic uranium ore has been extracted from the first and third orebodies at ERARM, there will remain approximately 100 million tonnes of tailings, waste material, and sub-economic grade ore. There are numerous alternatives for long-term containment of this material, one option is the creation of a 4 square kilometre, 17 metre high landform, termed the "above ground option" (Willgoose and Riley, 1993). Any surface landform configuration will be subjected to considerable erosion due to extremes of temperature and erosive rainfall.

Willgoose and Riley (1993) identified both short and long term possible erosion hazards which could be experienced after the cessation of mining at ERARM;

- Sediment influx into the local fluvial system from short-term erosion of waste rock material, and
- Radioactive and heavy metal contamination from long-term erosion of the tailings dam.

1.3 Research Objectives

Hydrological and geomorphological studies have been previously conducted by the Erosion and Hydrology Section of *eriss*, to ascertain reasonable estimates of erosion rates that the rehabilitated landform would experience over time. Studies have occurred on both the Northern Waste Rock Dump (NWRD) of ERARM (Willgoose and Riley, 1993; Saynor, Evans, Smith, and Willgoose, 1995; and Evans, Saynor and Riley, 1996) and in the Tin Camp Creek area (Moliere, Evans, Riley, and Willgoose, 1996). Tin Camp Creek, a tributary of the East Alligator River, is situated approximately 25 kilometres south west of Nabarlek (Figure 1.1.1).

Riley (1992; cited in Moliere *et al*, 1996) noted that weathering studies conducted on the NWRD may not reflect the long-term erosion rate of the landform, as the surfaces are relatively immature, having only had 5 to 8 years of exposure. Another more mature surface was sought that would reflect the state of the weathered waste rock material after a considerable time period. Uren (1992; cited in Moliere *et al*, 1996) stated that the Tin Camp Creek site would most likely reflect the erosional characteristics of a rehabilitated (including re-vegetation) structure at ERARM in the long term.

The current investigation involved similar hydrological and geomorphological studies as previously conducted at Tin Camp Creek and on the NWRD. Natural rainfall event monitoring on a 600 square metre field plot adjacent to Pit No. 1, at ERARM was conducted over the 1996/1997 wet season and constitutes the current project. It should be noted that the current study is also referred to as the natural site.

Willgoose (pers. comm.) noted that the three studies previously mentioned could be considered on a geological time-scale. Willgoose emphasised that the NWRD has been exposed for approximately ten years and represents the virtually unweathered nature of the waste rock material.

Evans, Riley, and Willgoose (1993; cited in Moliere *et al*, 1996) noted that the Tin Camp Creek site was assumed to represent waste rock material after at least 1,000 years of weathering and the development of natural vegetation.

Willgoose (pers. comm.) considered the natural site to represent waste rock material after approximately 10,000 to 100,000 years of weathering and the development of natural vegetation. Figure 1.3.1 highlights the three studies with respect to a geological time scale.

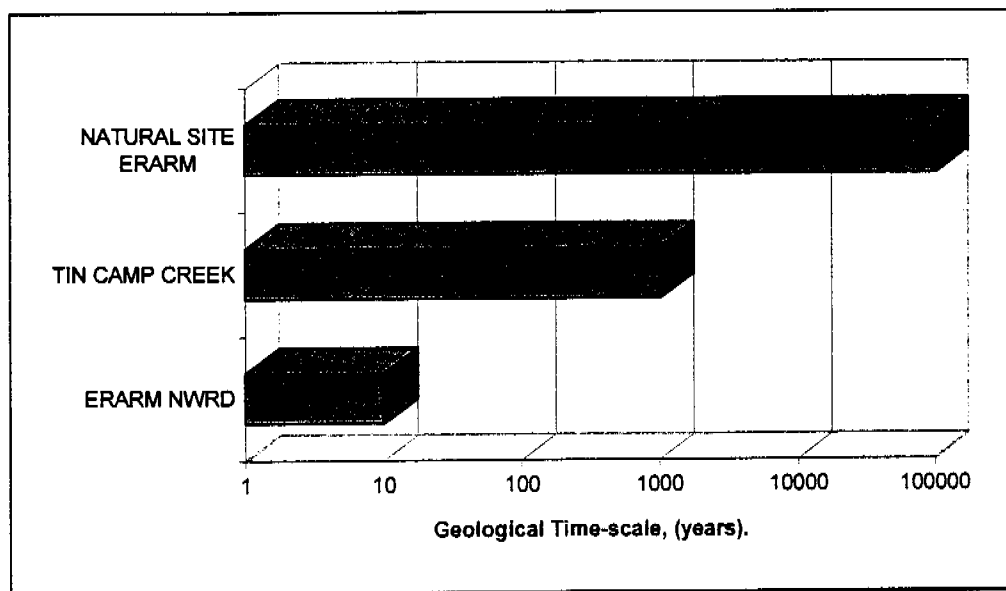


Figure 1.3.1: Each study listed is assumed to represent the weathered state of waste rock material after a certain number of years of exposure.

The specific research objectives of this study were;

- 1) Establishment of an erosion and runoff plot adjacent to Pit No.1 in undisturbed bushland;
- 2) Field monitoring on the plot by collecting rainfall, sediment (suspended and bedload) loss, and runoff data under natural rainfall.

- 3) Hydrological data collected was to be used to determine Distributed Field Williams (DISTFW) (Willgoose, Kuczera, and Williams, 1995) rainfall-runoff model parameters; and
- 4) Sediment loss data collected was to be used to determine parameters in sediment transportation equations from the landform evolution model, SIBERIA (Willgoose, Bras, and Rodriguez-Iturbe, 1989).

The DISTFW-NLFIT package (Willgoose *et al*, 1995) utilised in this study incorporates the DISTFW rainfall-runoff model with the nonlinear Bayesian regression analysis package, NLFIT (Kuczera, 1989). The package is able to estimate values for Field Williams hydrology model parameters that describe a discharge hydrograph. This hydrograph is calibrated to an observed hydrograph for a given rainfall event.

The landform evolution model, SIBERIA, is a computer model that can be used to predict the erosional development of catchments and their channel networks over time (Willgoose and Riley, 1993). Figure 1.3.2 illustrates the possible state of the post-mining rehabilitation structure after 1000 years of simulated erosion utilising SIBERIA.

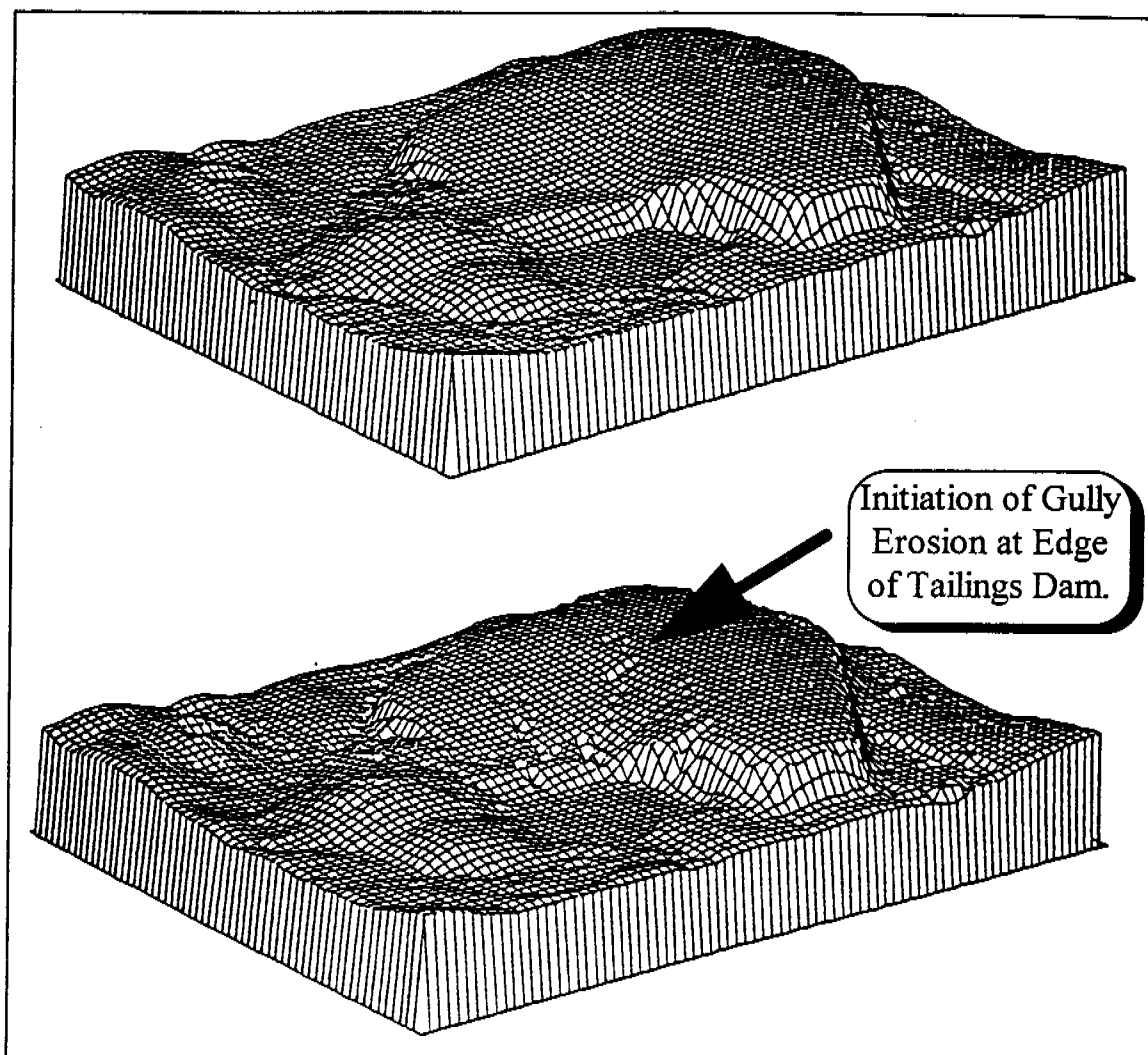


Figure 1.3.2: The 4 square kilometre, 17 metre high post-mining rehabilitation structure prior to erosion commencement is featured at the top of this Figure. Featured at the bottom of this Figure is the landform after 1000 years of simulated erosion by SIBERIA (after Willgoose and Riley, 1993). The initiation of gully erosion is also highlighted in this Figure.

It can be observed in the lower DTM plot of the rehabilitated landform (highlighted by a large arrow in Figure 1.3.2), that gully erosion is predicted to occur. The breach of the tailings dam wall and the subsequent release of radioactive and heavy metal tailings from gully erosion, was identified by Willgoose and Riley (1993) as a potential threat to the surrounding environment in the long term.

Over a geological time scale (Figure 1.3.2), SIBERIA simulates the erosional evolution of the rehabilitation structure. Over such a long period of time, rates of erosion are going to change, through the development of vegetation cover and changes in the physical composition of the erodible material. It is therefore important to compare the similarity of the natural site and the Tin Camp Creek site with respect to infiltration properties, to ascertain whether a long term trend in hydrologic behaviour is likely to exist, which may affect the erosion rates predicted by SIBERIA. A comparison between the predicted rates of sediment transportation utilising the overland flow erosion model and the total sediment loss model, from studies on the NWRD, in the Tin Camp Creek area, and the on the natural site is presented in Section 4.0.

Other minor objectives of the current study include the evaluation of the effect of vegetation growth on the hydrological characteristics of the field plot during the course of the wet season (Section 5.0). Previous studies (George, 1996) have been conducted to evaluate the effect of vegetation growth on a ripped, topsoiled site on the NWRD of ERARM. An evaluation of the deficiencies of the use of the least squares error model has also been conducted (Section 3.0). In a complex hydrologic model such as DISTFW, most of the distributions of errors in data sets violate the assumptions of the least squares model indicating that a more general error model should be used. The DISTFW-NLFIT package incorporates diagnostic statistics to assess the violations of least square error model assumptions and enables the selection of the appropriate form of a more general error model (Box-Cox transformation or an Auto-Regressive Moving Average) for a particular data set.

2.0 Rainfall-Runoff Experimental Field Plot

2.1 General Overview

Hydrology and sediment loss data was collected from a 600 square metre rainfall-runoff plot purposefully constructed in undisturbed bushland approximately 50 metres from the edge of Pit No.1, ERARM (Figure 2.1.1).

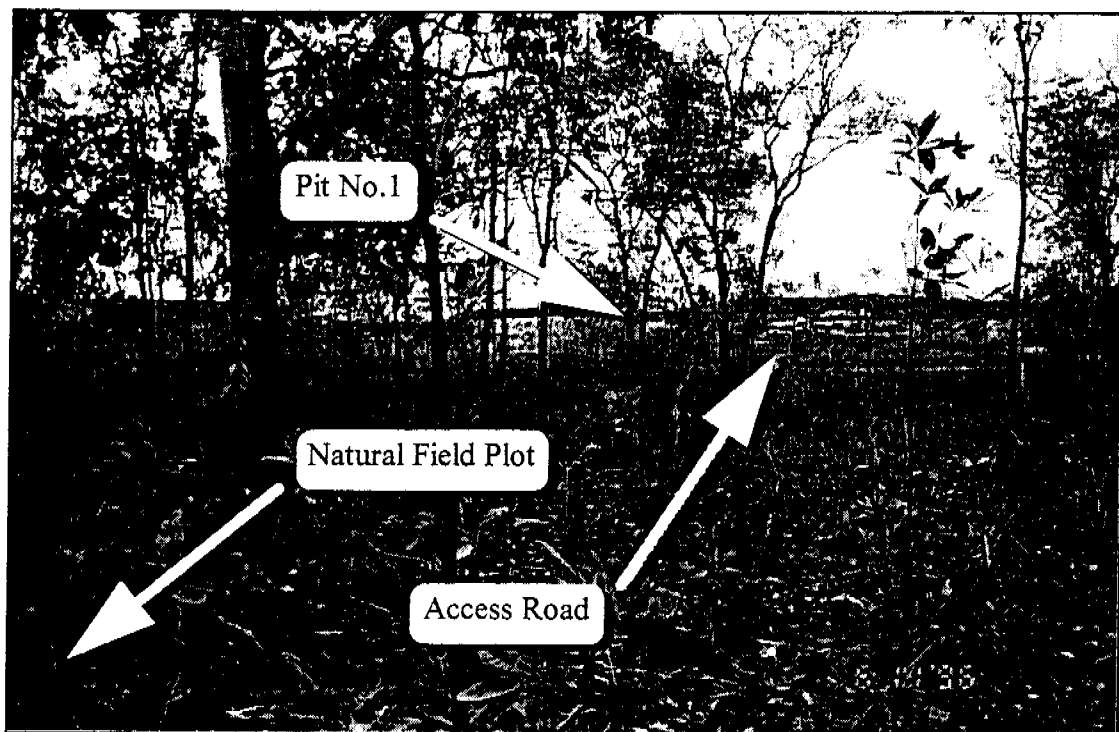


Figure 2.1.1: The undisturbed natural field plot is approximately 50 metres from the edge of Pit No. 1, ERARM. The *eriss* staff member featured in the background of this Figure, is standing along the access road.

Figure 2.1.1 illustrates the undisturbed character of the field plot area, prior to construction in early November 1996. The large open space in the background of Figure 2.1.1, is Pit No.1 which is approximately 700 metres in diameter. The vegetative ground-cover in the area is sparse to non-existent prior to the commencement of the monsoonal wet season.

The determination of the position of the field site involved meeting a number of criteria;

- The site had to be totally undisturbed, containing original vegetation;
- The site was not to be unduly sheltered from surrounding landform structures, such as the Southern Waste Rock Dump (SWRD);
- The general slope of the site must be conducive to the establishment of an experimental field plot; and
- The site must be representative of the landscape present before the commencement of mining operations.

The position of the field plot with respect to the SWRD, and Pit No.1, is illustrated in Figure 2.1.2.

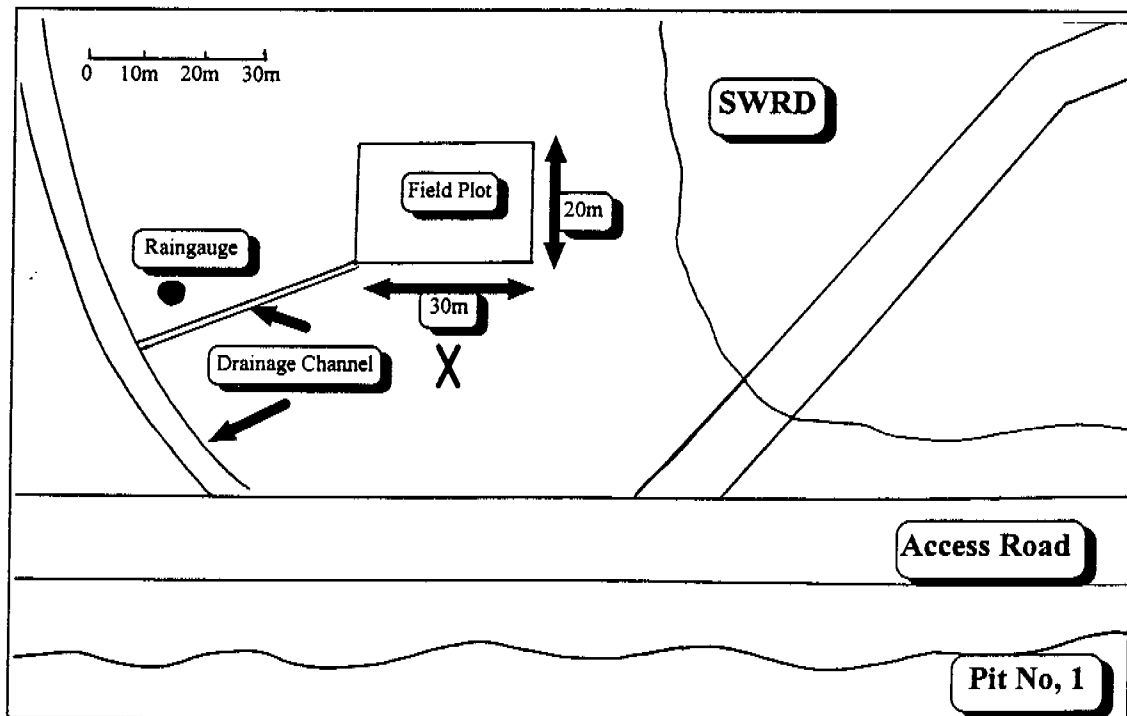


Figure 2.1.2: Schematic diagram highlighting the position of the field plot relative to the SWRD, Pit No.1, and the access road. The large cross, indicates the position of Figure 2.1.1. The position of the drainage channel and raingauge that were installed during the monitoring program are also featured in this Figure.

It can be observed from Figure 2.1.1 that the criteria that the plot should contain undisturbed vegetation was satisfied. Figure 2.1.2 highlights that the position of the field plot is sufficiently distant from the 15 metre high SWRD. The SWRD was not believed to have any notable shadowing effects upon rainfall falling upon the site. The vegetative characteristics of the field plot, were considered to be representative of other portions of undisturbed bushland around and outside the confines of ERARM.

The general topography of the field plot was ascertained in a survey using a TopCon total station theodolite (Figure 2.1.3). The average slope was calculated to be 0.027 metre drop per metre, thus satisfying the criteria of a gently sloping field plot.

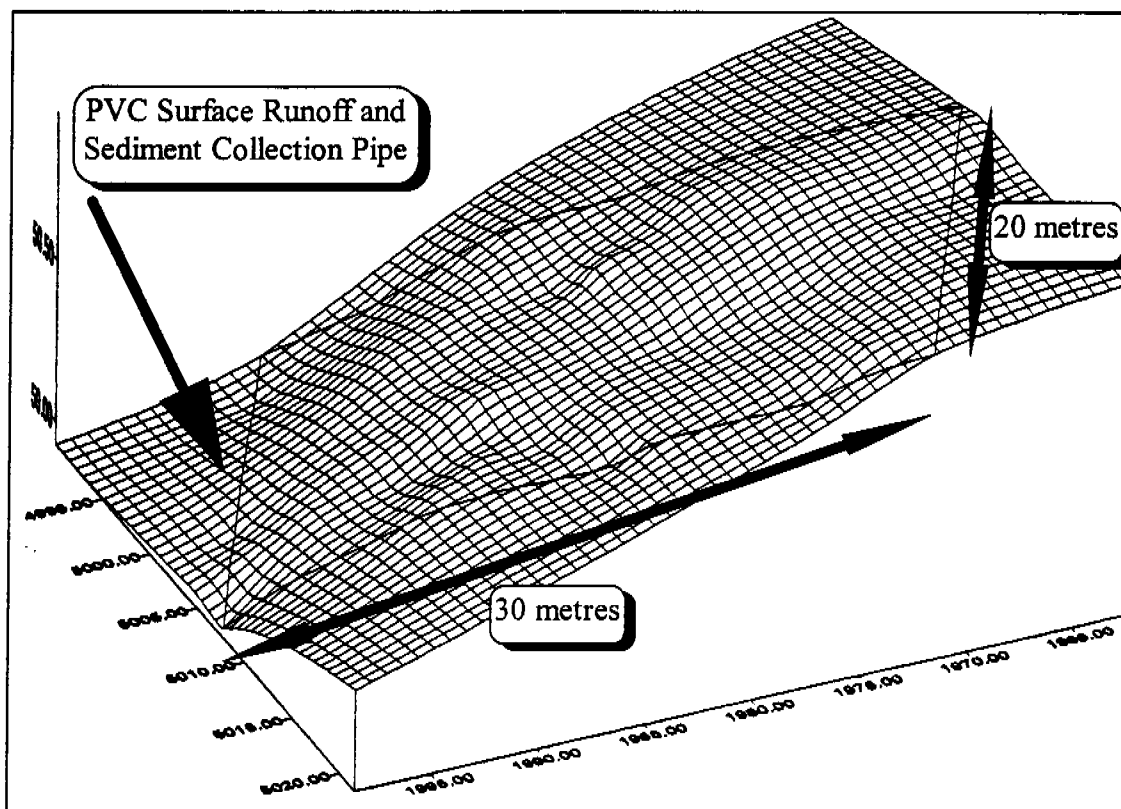


Figure 2.1.3: Three dimensional topographic surface of the 30m by 20m erosion and hydrology field plot which collected both surface run-off and transported sediment at the downslope end of the plot with a 300mm diameter PVC pipe. The dimension listed on the x, y, and z axes are a function of the computer program and are only relative to each other.

2.2 Experimental Field Plot

The 20 metre by 30 metre rainfall-runoff plot was hydraulically isolated from the surrounding bushland with damp-coarse, a bituminous coated aluminium building material. The material was approximately 20 centimetre wide, and a 5 centimetre section was bent at 90° and secured to the ground with large nails. The flattened edge of the material was set in place with concrete (Figure 2.2.1).

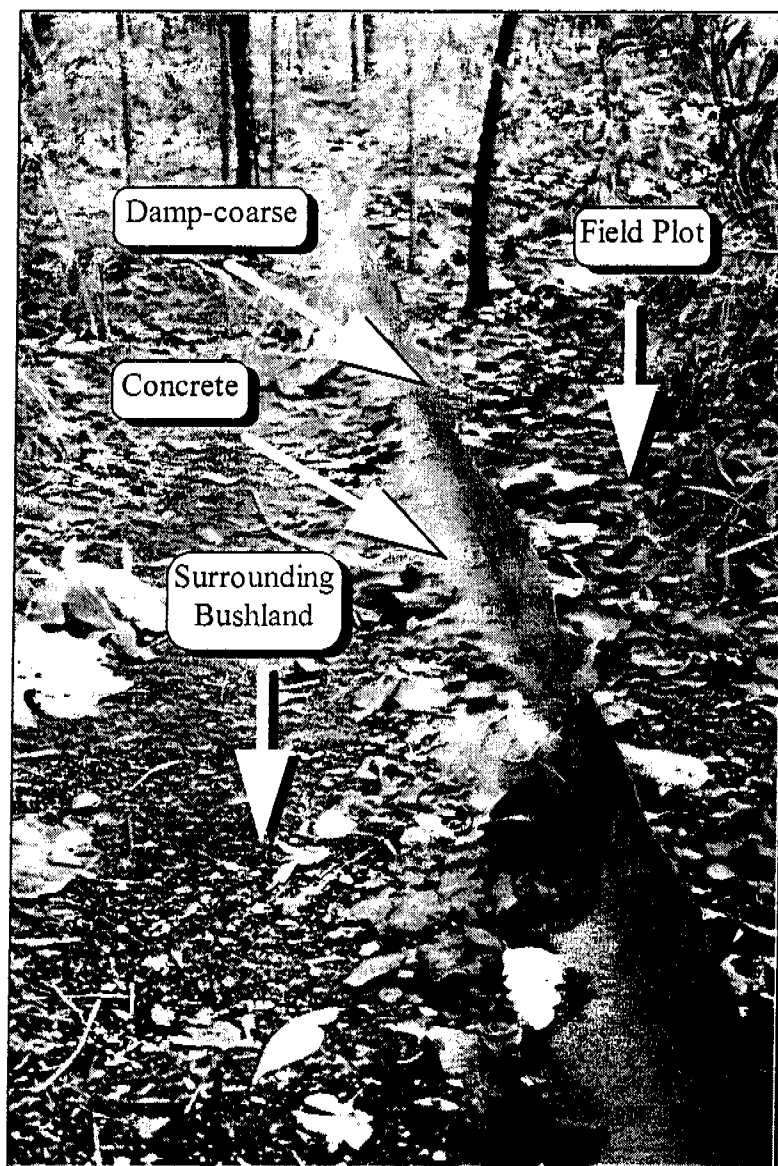


Figure 2.2.1: The 20 cm wide bituminous aluminium building product, (damp-coarse), was bent in a letter 'L' shape, and nailed to the soil surface, and supported with concrete. The field plot was thus hydraulically isolated from the surrounding bushland.

The damp-coarse material prevented the ingress of surface overland flow from the surrounding bushland. Sub-surface flow was not considered to be significant source of water.

The position of the field plot was purposefully chosen such that the general topography featured decreasing elevation (Figure 2.1.3). One half of a large PVC drainage pipe was buried into the ground at the down-slope end of the plot for the collection of surface run-off and sediment that was transported by the surface run-off.

The PVC pipe was 300 millimetres in diameter and 20 metres in length, and was donated by ERARM for the experiment. Figure 2.2.2 illustrates the downslope end of the field plot where the PVC pipe was installed.

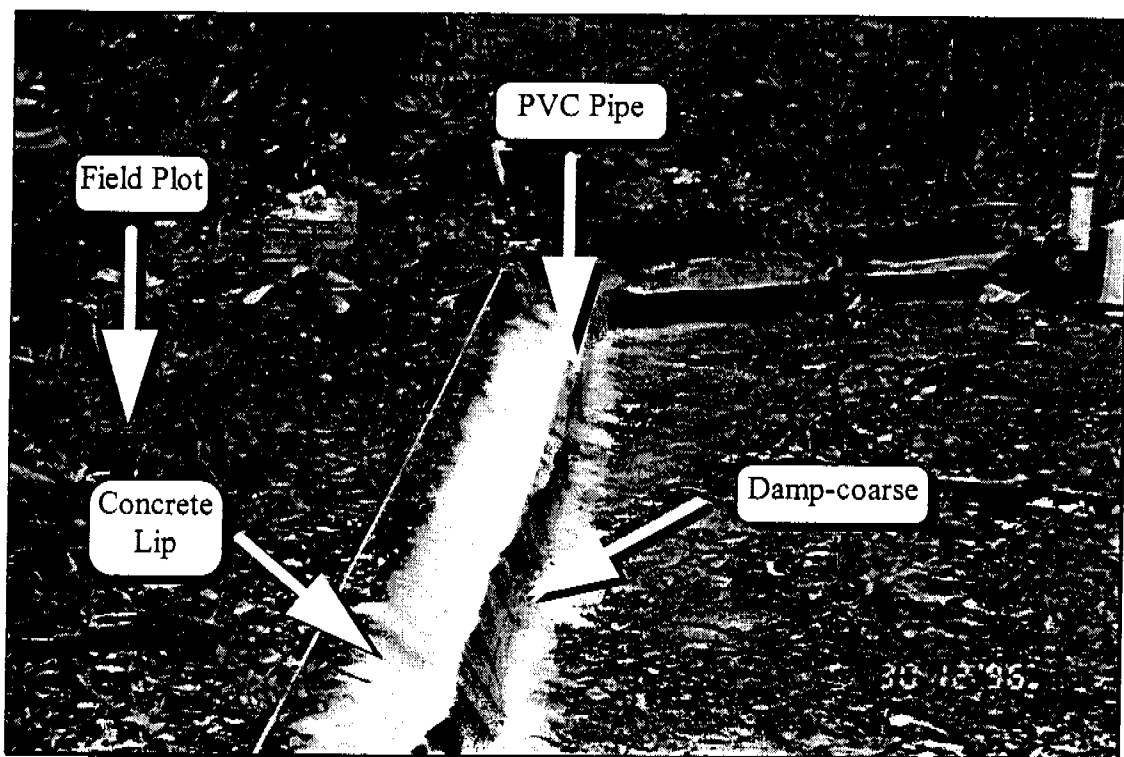


Figure 2.2.2: One half of a 300 mm diameter, 20 m long PVC pipe was buried at the down-slope end of the field plot. Additional damp-coarse material was attached to the PVC pipe to prevent overflow of surface runoff. A concrete lip was installed to allow unhindered transport of sediment and surface runoff into the PVC pipe.

The PVC pipe served a dual purpose, to conduct surface run-off from the plot and to provide temporary storage for sediment transported by that surface run-off. The nature of the installation of the half PVC pipe, buried at an angle, necessitated the construction of a concrete lip on the field plot side of the pipe for a smooth transition between the field plot and the pipe (Figure 2.2.2). Extra damp-coarse material was added to the right hand side of the PVC pipe (Figure 2.2.2), to prevent surface runoff from overflowing out of the pipe. During construction and rainfall event monitoring of the field plot, the ground surface was disturbed as least as possible. Figure 2.2.3 illustrates the concrete reservoir and hydraulic control structure which was visible in the background of Figure 2.2.2.

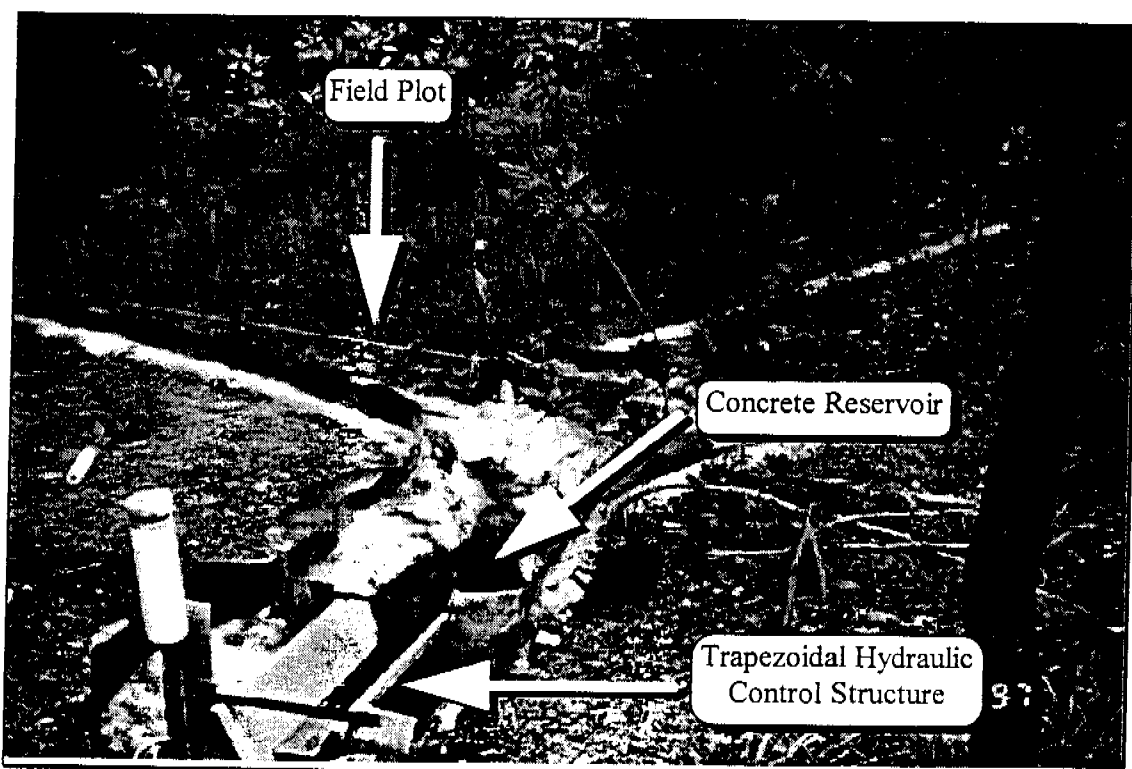


Figure 2.2.3: Featured in the foreground is the trapezoidal hydraulic control structure which was connected to a concrete reservoir which accumulated sediment, and partially controlled the run-off.

The concrete reservoir (Figure 2.2.3), collected bedload sediment that was swept into the PVC pipe from the plot and steadied the flow entering the trapezoidal hydraulic control structure. The concrete reservoir was hydraulically sealed with slight imperfections in the walls of the reservoir being filled with marine silicon sealant. The reservoir had an approximate volume of 20 litres.

Figure 2.2.4 illustrates the concrete reservoir after the cessation of a natural rain event. The turbulent water, highlighted by the large arrow to the left of Figure 2.2.4, is surface run-off flowing from the PVC pipe into the reservoir.

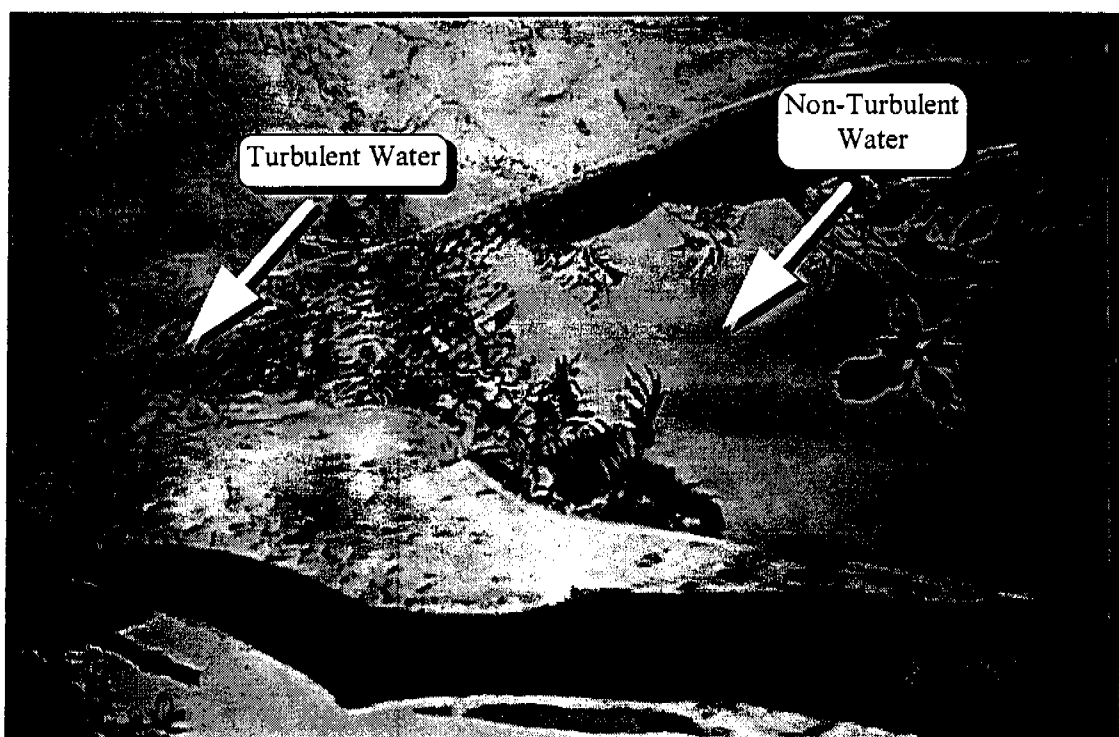


Figure 2.2.4: The concrete reservoir served a dual purpose; to collect bedload sediment that was transported during rain events and steady the flow entering the hydraulic control structure. Surface runoff that is leaving the PVC pipe, (highlighted by an arrow to the left of the Figure), enters the concrete reservoir and is quickly steadied, (highlighted by an arrow to the right of the Figure).

The reservoir was rectangular in plan view, with the PVC pipe supplying water at one end, highlighted by an arrow to the left of Figure 2.2.4. Figure 2.2.5 illustrates a cross-sectional schematic of the flow steadying ability of the reservoir trapezoidal weir system.

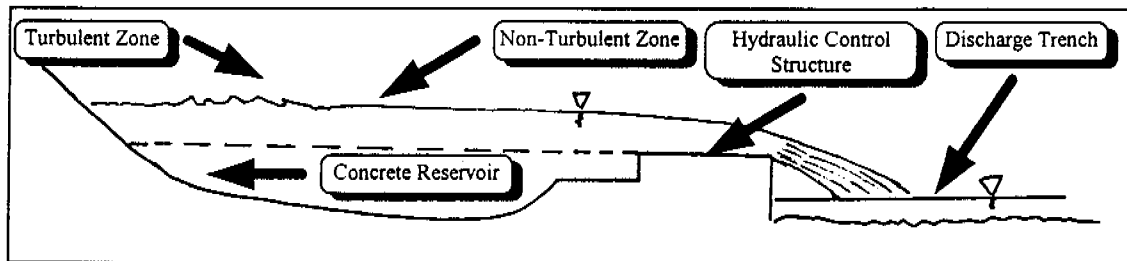


Figure 2.2.5: The concrete reservoir serves to steady the flow of water across the hydraulic control structure, and as a storage area for bedload sediment.

Figure 2.2.6 illustrates the behaviour of the reservoir and control structure system during large storm activity.

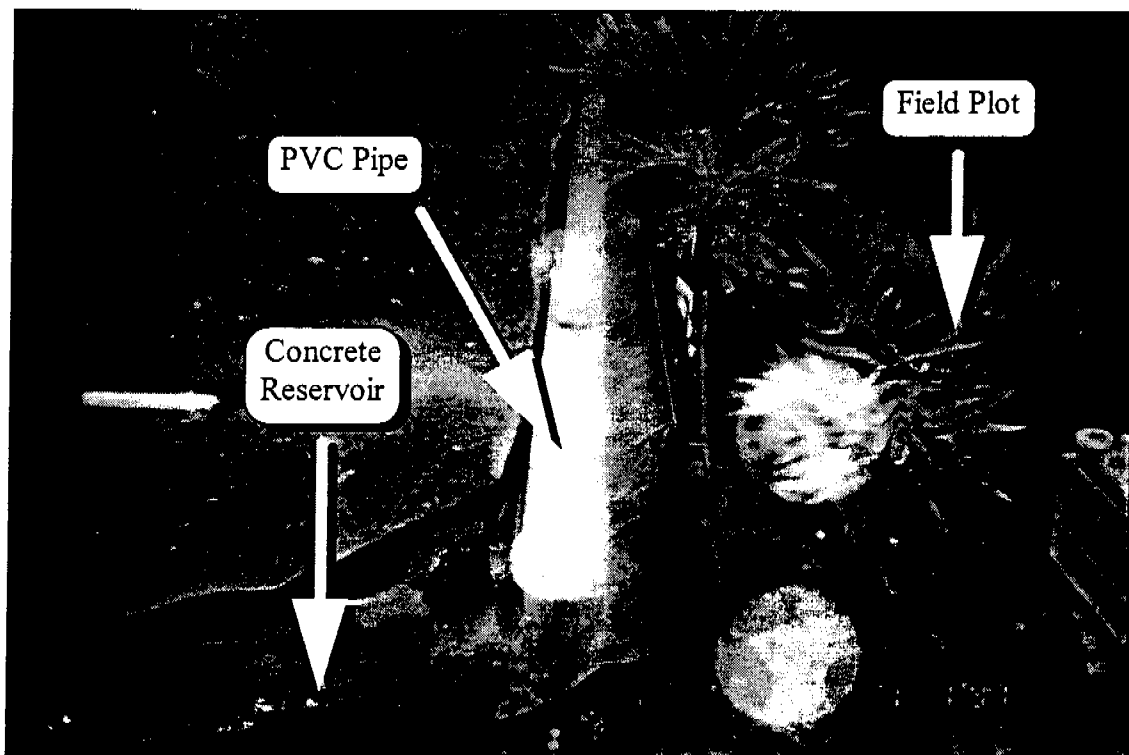


Figure 2.2.6: Considerable quantities of surface run-off are transported from the field plot, the change in direction of flow, and the length of the reservoir both serve to control and steady the flow.

The water level in the reservoir was refilled before the commencement of each monitored storm event, so that any initial surface run-off occurring could be recorded accurately by the control structure. The discharge trench featured in Figures 2.1.1 and 2.2.5, comprised of a large ditch dug out roughly with a back-hoe, (ERARM), to allow run-off from the experimental area to be transported away.

The trapezoidal hydraulic control structure installed following the concrete reservoir, provided a method for the determination of the quantity of discharge, via a water level height measurement. The control structure utilised in this study was a “150 mm RBC flume” (Bos *et al*, 1984; cited in Evans and Riley, 1993) and was constructed of galvanised steel. Figure 2.2.7 illustrates a cross-sectional view of the RBC flume.

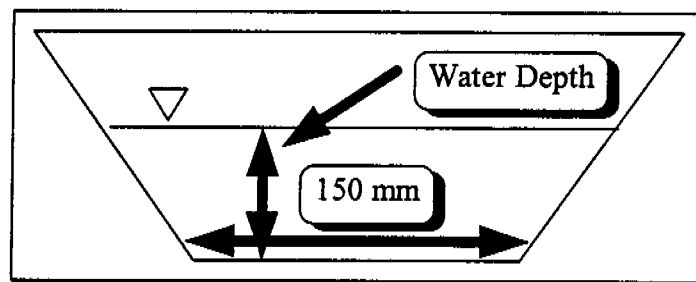


Figure 2.2.7: Cross-sectional view of the hydraulic control structure, with a base of 150 mm. The depth of water, with respect to cross-sectional area, is utilised to determine the discharge through the structure.

The relationship between the depth of water, ‘h’, (m), and the quantity of discharge , ‘Q’, (m³/s), was previously determined (Equation 2.2.1), (Evans and Riley, 1993).

$$Q = 18.4 \times h + 940 \times h^2 \quad (r^2 = 1) \quad (2.2.1)$$

where

Q = Discharge, (m³/s), and

h = Depth of water, (m).

Figure 2.2.8 illustrates the trapezoidal control structure, the concrete reservoir, the discharge trench, and the water level sensing probe, termed a capacitance rod.

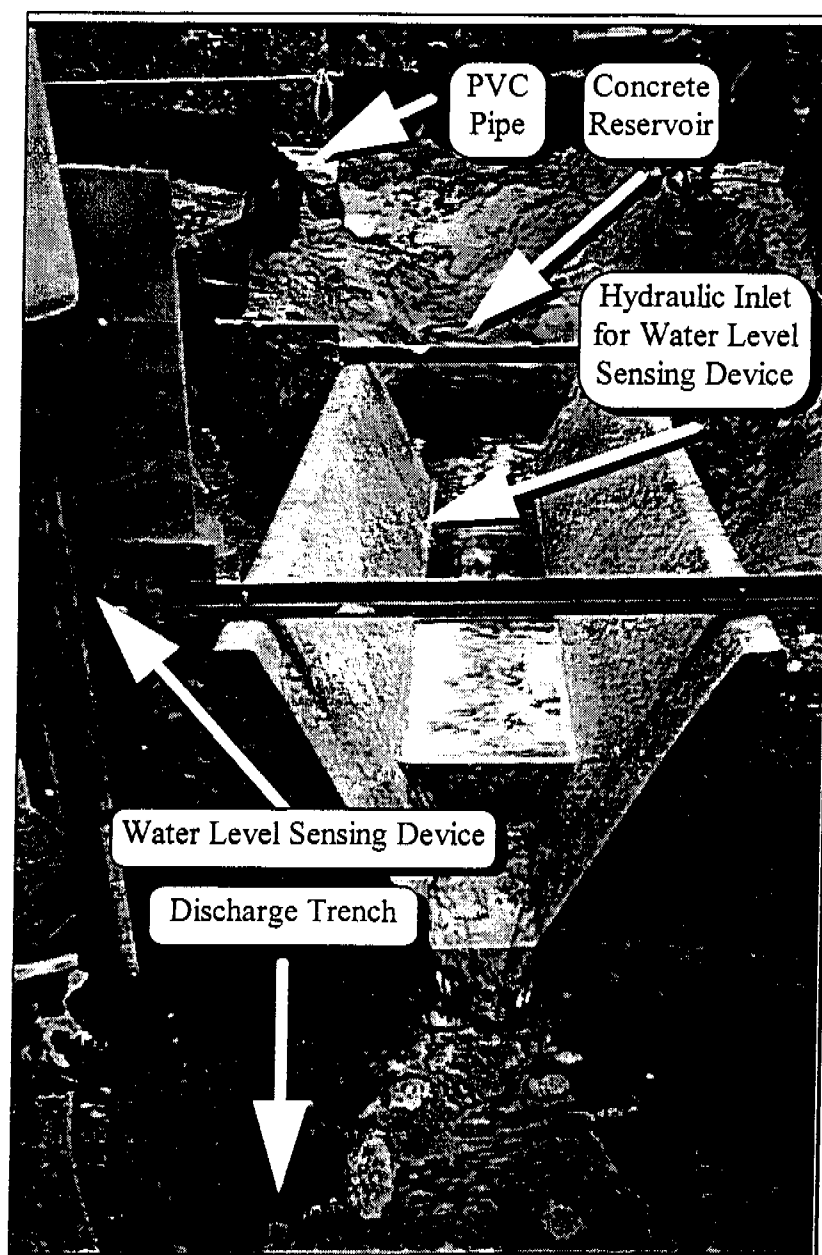


Figure 2.2.8: Run-off is still occurring in the foreground of this Figure after a storm event. The position of the hydraulic inlet that is connected to the stilling well containing the water level sensing device is also featured in this Figure.

It was generally observed that for a considerable period of time after the cessation of rainfall, surface run-off continued to occur (Figure 2.2.8). Surface run-off flowing from the control structure is directed into the discharge trench and carried away from the site (Figures 2.1.1, and 2.2.5).

In the left foreground of Figure 2.2.8, a small section of white PVC stormwater pipe sits atop a small clear plastic cylinder, termed a stilling well. The stilling well contained the water level sensing probe, which had an insulated core that was wrapped with a thin, bare wire. Minute changes in resistance, detected by the connected electronic data logger, due to more or less of the bare wire contacting water within the stilling well, yielded a measurement of the water level. The relative resistance reading was stored by the data-logger along with a time signature. The stilling well housing the sensor, was hydraulically connected to the base of the control structure (Figure 2.2.8). Manual water level readings were taken using a measuring tape attached to side of the stilling well. The water within the stilling well was coloured with a fluorescent dye for ease of reading.

The DISTFW rainfall-runoff model required input of information pertaining to the topography of the catchment, and time related discharge and rainfall data. Rainfall data was recorded utilising an electronic and a manual raingauge, that were positioned approximately 20 metres from the field plot (Figure 2.2.9).

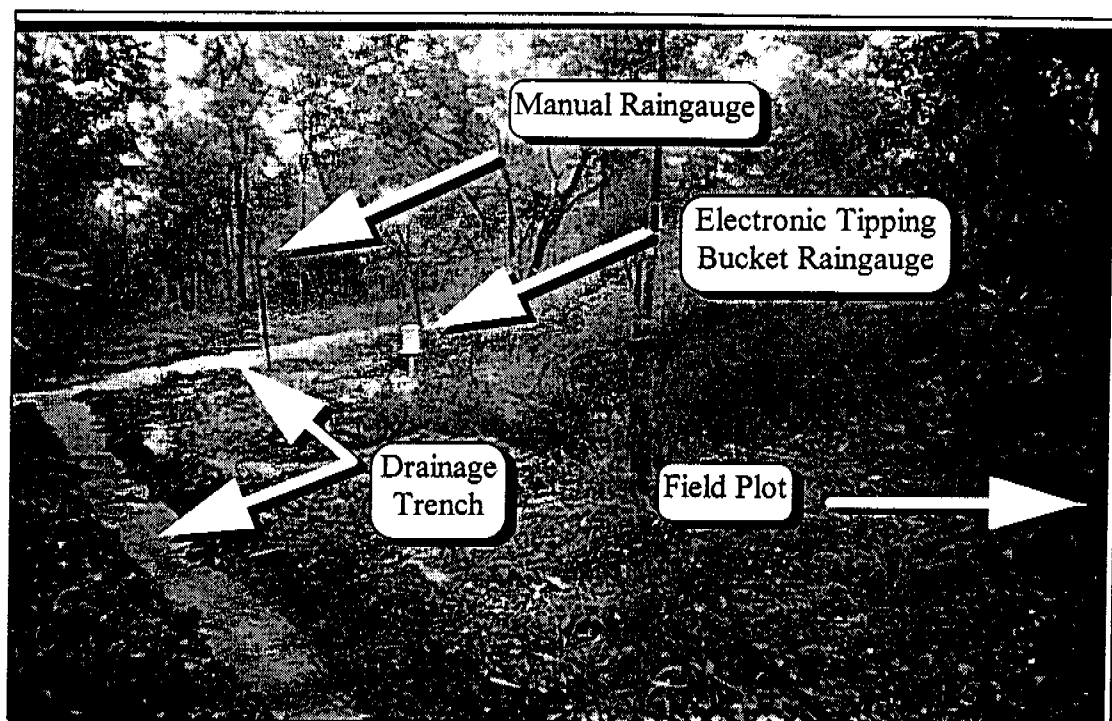


Figure 2.2.9: Featured to the left of this Figure is the discharge trench that was constructed to carry runoff away from the experimental area. Attached to the star picket in the background of this Figure is the manual raingauge, and the steel cylinder sitting atop a pedestal, in the middle of the Figure, is the electronic tipping bucket raingauge.

The electronic tipping bucket raingauge consisted of two L-shaped plastic buckets (in a back to back formation) that held 0.2 mm of rainfall each; a magnet; and a magnetic sensitive switch. When 0.2 mm of rainfall accumulated in one L-shaped bucket, from the feed mechanism, the two bucket mechanism pivoted via a fulcrum, and emptied one bucket, and the other bucket began to fill. A magnet was attached to the base of the two L-shaped buckets and tripped a magnetic sensitive switch when the buckets moved. Signals from the magnetic switch were recorded by a connected data logger. Figure 2.2.10 presents a schematic of a typical electronic tipping bucket raingauge.

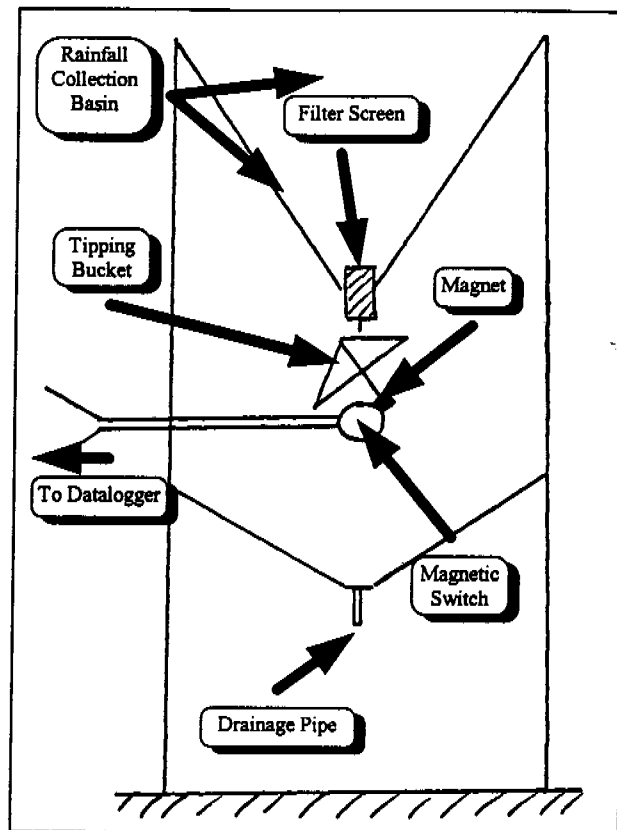


Figure 2.2.10: A schematic of a tipping bucket raingauge featuring two L-shaped plastic buckets in a back to back configuration attached to a fulcrum, a magnet attached to the plastic bucket mechanism, and a magnetic sensitive switch which was connected to an electronic data logger.

The filter screen featured in Figure 2.2.10 at the base of the collection basin, ensured the exclusion of leaves and twigs from the raingauge. The tall vegetation surrounding the electronic raingauge (Figure 2.2.9), was partially cleared to ensure that the gauge was not shadowed. The electronic data-logger recorded the cumulative tip number along with a time signature. Manual rainfall data was collected in a NYLEX "1000" plastic rain-gauge which was factory calibrated to allow direct readings of rainfall in millimetre increments.